Kinematic and Dynamic Analysis of Two Link Robot Arm using PID with Friction Compensator

Kaung Khant Ko Ko Han, Aung Myo Thant Sin, Theingi

Abstract— This paper presents a position controller that is used in each joint of two links robot arm. Kinematics and dynamic analysis of two link robot arm are reported by modelling in a vertical movement. A complete derivation of the Newton-Euler method and Lagrange-Euler are studied. Corresponding joint torques computed in each time step are plotted. The robot arm is control for desired trajectory by using PID (proportional, integral and derivative) with friction compensator. PID is applicable in many control problems, but due to its large error in position control system. To solve this problem, the position controller is composed of conventional PID and model-based friction compensation. The proposed (PID plus friction compensator) controller minimize the position error in set point control and trajectory tracking control, and thus, improve the stability. The friction compensator is integrated with static friction, Coulomb friction, viscous friction and Stribeck effect. A prototype is presented with metal links and servo motors.The proposed control scheme was tested using two links robot arm.

Index Terms— Proportional-Integral-Derivative (PID), Two Link Robot Arm, Rate-Dependent Friction, 2 DOF Robot Manipulator.

———————————— ◆ ————————————

1 INTRODUCTION

RECENT years, robotics and mechatronics had developed in industrial, walfare and medical techonology and bring a lot of benefit. Different types of exoskeleton and rehabilitation devices are used in medical and daily living activities. These devices can help the person in many individual works and recreational activities. Many kinds of control strategies [1], [2], [3] appear among the different types of exoskeleton and have been proposed in some survey papers and related papers for exoskeleton and rehabilitation devices.

Parallel and serial robot arm play as an important role in those organization. The development in serial manipulator is advantageous for the researchers for its better control, singular configuration, improving workspace and optimization of the robot arm parameter. The important aspect of dynamic studies of the manipulator is to nature of robot arm behavior and magnitude of torque, singularity avoidance, power requirements and optimization criterion.

PD control with computed feed forward controller was compared and was found best computed-torque control, PD control with computed feed forward and PD control based on root mean square average performance index [4]. An alternative solution of Artificial Neural Network method for forward and inverse kinematic mapping was proposed [5]. The decoupling of dynamic equations eliminates torques caused by gravitational, coriolis forces and centripetal [6]. Kinematic and dynamic parameters are analyzed using ANNOVA to imitate the real time performance of 2-DOF planar robot arm [7]. Optimal

dynamic balancing is formulated by minimization of the root-mean-square value of the input torque of 2 DOF serial robot arm and experimental results are simulated using ADAMS software [8]. The dynamic parameters of 2 DOF are estimated as well as experimental results are validated through simulation [9]. Serially arranged n-link by non-linear control law is derived using Lyapunov-based theory [10]. Recently, position control using neuro-fuzzy controller is presented for 2 DOF serial manipulator [11].

In position control system, friction is the highly non-linear characteristics and it is difficult to model of its dynamic behaviours. However, appropriate friction model was choosed for prediction and compensation in suitable position control system. In recent years, friction model based on the classic friction model such as static friction, Coulomb friction, viscous friction and Stribeck effect.
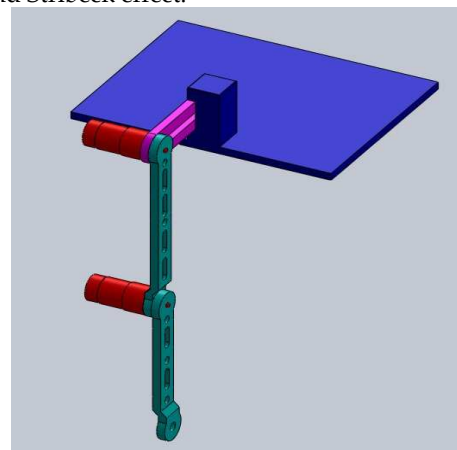

Fig. 1. Two Link Robot Arm (Isometric View)

This standalone friction model is combined to produce the appropriate friction model for example Tustin model [11]. Dahl model [12] was based on Coulomb friction model. LuGre [13] and generalized Maxwell slip (GMS) [14] also used static, Coulomb and Stribeck effect that can be expressed on static map between velocity and torque. Here, the friction compen-

————————————————
- *Kaung Khant Ko Ko Han is currently pursuing doctrorial degree program in mechatronic engineering depertment in Yangon Technological University, Myanmar, PH-09978954545. E-mail: kaungkhant.mce@gmail.com*
- *Aung Myo Thant Sin is a lecturer in mechatronic engineering depertment in Yangon Technological University, Myanmar, PH-09963866874. E-mail: nayaye1@gmail.com*
- *Theingi is currently Rector of Technological University- Thanlyin, Myanmar. E-mail: theingi.sa@gmail.com*

sation in proposed position controller was based on static, Coulomb, viscous models and Stribeck effect. From this static model can conduct to LuGre and generalized Maxwell slip (GMS). Model based friction compensation can be used in stimulation, gain tunning and stability analyse [16].

This paper concerns the kinematic and dynamic analysis of 2 link robot arm (see in Fig. 1) and PID controller with friction compensator. A two links robot arm's kinematics, and dynamic equations are obtained and dynamic analysis is the deriving equations, the relationship between force and motion in a system. The Newton-Euler method and Lagrange are derived completely. The corresponding joint torques computed in each time step are plotted and choosed the motor from aid of this result. The proposed (PID plus friction compensator) controller minimize the position error in set point control and trajectory tracking control, and thus, improve the stability. The friction compensator is integrated with static friction, Coulomb friction, viscous friction and Stribeck effect.

This report is organized as follows. Section 2 discusses the kinematic and section 3 is dynamic analysis. Section 4 is proposed position controller and fricition compensator. Section 5 is the experimental results. Section 6 & 7 are the discussion and conclusion.

2 KINEMATIC OF TWO LINK ROBOT ARM

Robot kinematics applies geometry to the investigation the movement of multi-degree of freedom kinematic chains that form the structure of robot arm.

2.1 Forward Kinematic

Given the joint angles and the links geometry, compute the orientation of the end effector involved in the execution of a movement is kinematic. A limb, as a mechanical device, converts muscle lengths and joint angles to hand positions. This process is referred to as forward kinematics. In Fig. 2, an idealized model of this transformation for movements in a vertical plane is illustrated. The arm is modeled as two rigid links of length 260 mm and 230 mm, the links rotate about horizontal parallel axes that are fixed with respect to the links. For this idealized model the forward kinematics from joint angles (θ_1, θ_2) to hand position (x, y) are given by

$$x = l_1 \cos(\theta_1) + l_2 \cos(\theta_1 + \theta_2) \qquad (1)$$

$$y = l_1 \sin(\theta_1) + l_2 \sin(\theta_1 + \theta_2) \qquad (2)$$

Given a desired hand position, choose the appropriate muscle lengths and corresponding joint angles to achieve that position. The transformation from desired hand position to the corresponding joint angles and muscle lengths is known as the inverse kinematic transformation. Internal models of arm kinematics are also useful in choosing torques at the joints of the arm to achieve a particular force and torque between the hand and some external object. Learning to move accurately may involve building internal models of kinematic transformations.
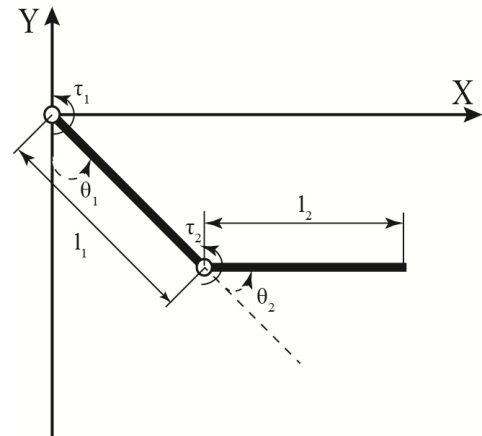

Fig. 2. Two Link Robot Arm for Forward Kinematic.

2.2 Inverse Kinematic

Given the position and orientation of the end effector relative to the base frame compute all possible sets of joint angles and link geometries which could be used to attain the given position and orientation of the end effector. The inverse kinematic transformation for the idealized two-joint robot arm model (Fig. 3) can be represented mathematically:

$$x^2 + y^2 = l_1^2 \cos^2(\theta_1) + l_2^2 \cos^2(\theta_1 + \theta_2) + 2l_1 l_2 \cos(\theta_1) \cos(\theta_1 + \theta_2) + \qquad (3)$$
$$l_1^2 \sin^2(\theta_1) + l_2^2 \sin^2(\theta_1 + \theta_2) + 2l_1 l_2 \sin(\theta_1) \sin(\theta_1 + \theta_2)$$

To control a two-joint robot arm, the inverse kinematic transformation could be implemented as a digital computer program as following:

$$\theta_2 = a\tan 2(\ \sin\theta_2, \cos\theta_2\ )$$

$$= a\tan 2(\ \pm\sqrt{1 - \cos^2\theta_2}, \cos\theta_2\ )$$

$$= a\tan 2(\ \pm\sqrt{1 - (\frac{x^2 + y^2 - l_1^2 - l_2^2}{2l_1 l_2})}, \frac{x^2 + y^2 - l_1^2 - l_2^2}{2l_1 l_2}\ )$$

$$(4)$$

$$\theta_1 = a\tan 2(y,x) - a\tan 2(k_2,k_1) \qquad (5)$$

Where

$$k_1 = l_1 + l_2 \cos\theta_2 \qquad (6)$$
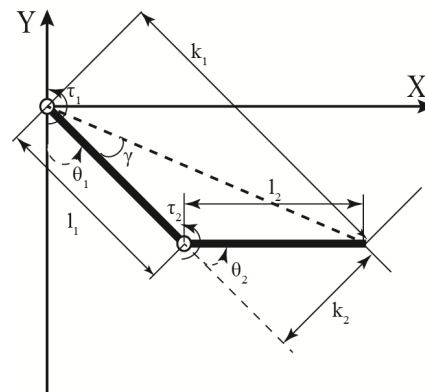
$$k_2 = l_2 \sin\theta_2 \qquad (7)$$

Fig. 3. Two Link Robot Arm for Inverse Kinematic.

3 DYNAMIC OF TWO LINKS ROBOT ARM

As demonstrated in this document, the numbering for sections upper case Arabic numerals, then upper case Arabic numerals, separated by periods. Initial paragraphs after the section title are not indented. Only the initial, introductory paragraph has a drop cap.

3.1 Lagrangian and Newton-Euler Formulations

It is necessary to analyze the dynamic characteristics of a manipulator in order to control it, to simulate it, and to evaluate its performance. A manipulator is most often an open-loop link mechanism, which may not be a good structure from the viewpoint of dynamics (it is usually not very rigid, its positioning accuracy is poor, and there is dynamic coupling among its joint motions). This structure, however, allows us to derive a set of simple, easily understandable equations of motion.

Two methods for obtaining the equations of motion are well known: the Lagrangian and the Newton-Euler formulations. At first the Lagrangian formulation was adopted. This approach has a drawback in that the derivation procedure is not easy to understand physically; it uses the concept of the Lagrangian, which is related to kinetic energy. However, the resulting equation of motion is in a simple, easily understandable form and is suitable for examining the effects of various parameters on the motion of the manipulator.

Recently, as the need for more rapid and accurate operation of manipulators has increased, the need for real-time computation of the dynamics equations has been felt more strongly. The Newton-Euler formulation has been found to be superior to the Lagrangian formulation for the purpose of fast calculation. Also, the Newton-Euler formulation is valid for computed torque control.

3.2 Lagrangian Formulation

We will derive the dynamics equation of a two-link robot arm movement. Let us consider the robot arm in Fig. 4. The following notations are used in the figure:

θ_i = the joint angle of joint-i,

m_i = the mass of link-i,

$\tilde{I}_i$ = the moment of inertia of link-i about the axis that passes through the center of mass and is parallel to the Z-axis, and
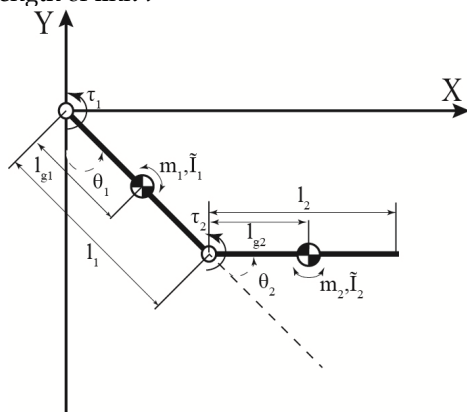
l_i = the length of link-i

Fig. 4. Dynamic Analysis of Two Link Robot Arm.

The following Fig. 5 is the front view of the experimental setup of the two link robot arm is drawing using the Solid-Wrok. The dimensions of the two link robot arm is expressed in following Table 1;

TABLE 1
DIMENSION OF THE 2-LINKS ROBOT ARM

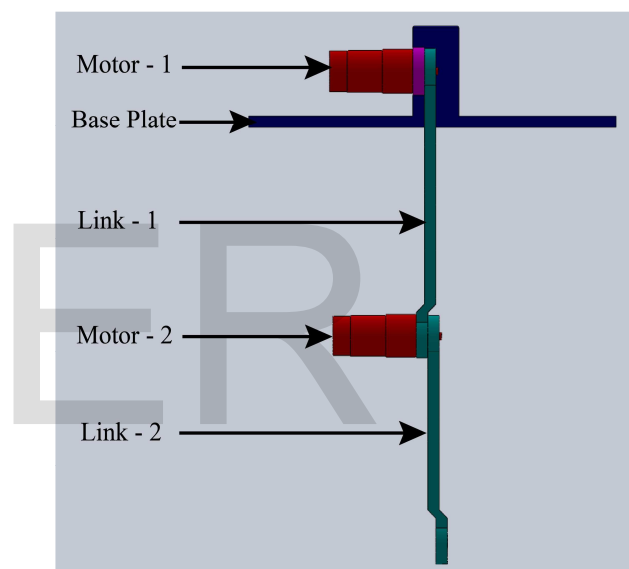| Parts of the Robot Arm	Dimension of the Parts
Link -1 (Length x Width x Thickness)	(260 x 30 x 10) mm
Link -2 (Length x Width x Thickness)	(230 x 30 x 10) mm
Diameter of Motor 1 and 2	38 mm
Shaft Diameter of Motor 1 and 2	6 mm
Base Plate (Length x Width x Thickness)	(250 x 200 x 10) mm

Fig. 5. Drawing for Two Link Robot Arm (Front View)

We assume that the first joint driving torque τ_1 acts between the base and link - 1, and the second joint driving torque τ_2 acts between links 1 and 2.

Choosing $q_1 = \theta_1$ and $q_2 = \theta_2$ as generalized coordinates, we will find the Lagrangian function. Let the kinetic energy and the potential energy for link - i be K_i and P_i respectively. For link - 1, we have

$$K_1 = \frac{1}{2} m_1 l_{g1}{}^2 \dot{\theta}_1{}^2 + \frac{1}{2} \tilde{I}_1 \dot{\theta}_1{}^2, \qquad (8)$$

$$P_1 = m_1 \hat{g} l_{g1} S_1, \qquad (9)$$

where $\hat{g}$ is the magnitude of gravitational acceleration. For link - 2, since the position of its center of mass $s_2 = [s_{2x}, s_{2y}]^T$ is given by

$$s_{2x} = l_1 C_1 + l_{g2} C_{12}, \qquad (10)$$

$$s_{2y} = l_1 S_1 + l_{g2} S_{12}, \qquad (11)$$

We have the relation

$$\dot{s}_2{}^T \dot{s}_2 = l_1{}^2 \dot{\theta}_1{}^2 + l_{g2}{}^2 (\dot{\theta}_1 + \dot{\theta}_2)^2 + 2 l_1 l_{g2} C_2 (\dot{\theta}_1{}^2 + \dot{\theta}_1 \dot{\theta}_2). \qquad (12)$$

Also,

$$K_2 = \frac{1}{2} m_2 \dot{s}_2^{\,T} \dot{s}_2 + \frac{1}{2} \tilde{I}_2 (\dot{\theta}_1 + \dot{\theta}_2)^2 \qquad (13)$$

and

$$P_2 = m_2 \hat{g}(l_1 S_1 + l_{g2} S_{12}). \qquad (14)$$

Calculating $L = K_1 + K_2 - P_l - P_2$ and the equations of motion for the two-link arm are:

$$\begin{aligned}
\tau_1 = & [m_1 l_{g1}^2 + \tilde{I}_1 + m_2(l_1^2 + l_{g2}^2 + 2l_1 l_{g2} C_2) + \tilde{I}_2] \ddot{\theta}_1 \\
& + [m_2(l_{g2}^2 + l_1 l_{g2} C_2) + \tilde{I}_2] \ddot{\theta}_2 - m_2 l_1 l_{g2} S_2 (2\dot{\theta}_1 \dot{\theta}_2 + \dot{\theta}_2^2) \\
& + m_1 \hat{g} l_{g1} C_1 + m_2 \hat{g}(l_1 C_1 + l_{g2} C_{12}),
\end{aligned} \qquad (15)$$

$$\begin{aligned}
\tau = & [m_2(l_{g2}^2 + l_1 l_{g2} C_2) + \tilde{I}_2] \ddot{\theta}_1 + (m_2 l_{g2}^2 + \tilde{I}_2) \ddot{\theta}_2 \\
& + m_2 l_1 l_{g2} S_2 \dot{\theta}_1^2 + m_2 \hat{g} l_{g2} C_{12}.
\end{aligned} \qquad (16)$$

This can also be rewritten as

$$\tau_1 = M_{11} \ddot{\theta}_1 + M_{12} \ddot{\theta}_2 + h_{122} \dot{\theta}_2^2 + 2h_{112} \dot{\theta}_1 \dot{\theta}_2 + g_1, \qquad (17)$$

$$\tau_2 = M_{21} \ddot{\theta}_1 + M_{22} \ddot{\theta}_2 + h_{211} \dot{\theta}_1^2 + g_2, \qquad (18)$$

Where,

$$M_{11} = m_1 l_{g1}^2 + \tilde{I}_1 + m_2(l_1^2 + l_{g2}^2 + 2l_1 l_{g2} C_2) + \tilde{I}_2, \qquad (19)$$

$$M_{12} = M_{21} = m_2(l_{g2}^2 + l_1 l_{g2} C_2) + \tilde{I}_2, \qquad (20)$$

$$M_{22} = m_2 l_{g2}^2 + \tilde{I}_2, \qquad (21)$$

$$h_{122} = h_{112} = -h_{211} = -m_2 l_1 l_{g2} S_2, \qquad (22)$$

$$g_1 = m_1 \hat{g} l_{g1} C_1 + m_2 \hat{g}(l_1 C_1 + l_{g2} C_{12}), \qquad (23)$$

$$g_2 = m_2 \hat{g} l_{g2} C_{12}. \qquad (24)$$

Inverse dynamic analysis has been done for the joint space spiral trajectory considered for the controller design. Fig. 6, Fig. 7, Fig. 8 illustrate the driving torques (τ1, τ2) of the 2 link manipulator from the knowledge of the trajectory equation in terms of time. The following simulation result is based on Lagrange Formulation.

In Fig. 6, dynamic analysis of 2 links robot arm and q(1) (Joint 1 angle) is setting 0 to 30 degree and q(2) is setting 30 to 60 degree. The initial torque for joint - 1 is near 1.4 N-m and joint – 2 is about -0.225 N-m.

In Fig. 7, dynamic analysis of 2 links robot arm and q(1) (Joint 1 angle) is setting 0 to 90 degree and q(2) is setting 90 to 180 degree. The initial torque for joint - 1 is near 1.4 N-m and joint – 2 is about -0.225 N-m.
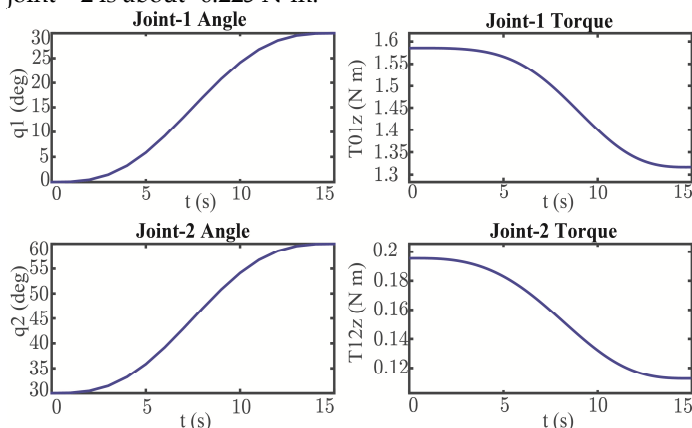

Fig. 6. Dynamic Analysis of Two Links Robot Arm, q(1) = 0 ~ 30 degree and q(2) = 30 ~ 60 degree
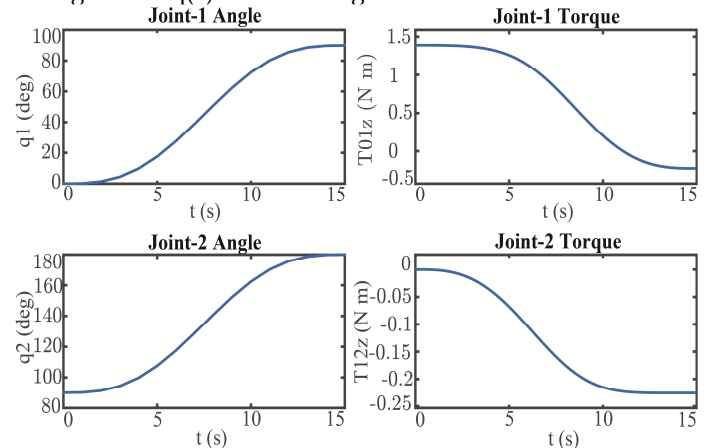

Fig. 7. Dynamic Analysis of 2-Links Robot Arm, q(1) = 0 ~ 90 degree and q(2) = 90 ~ 180 degree

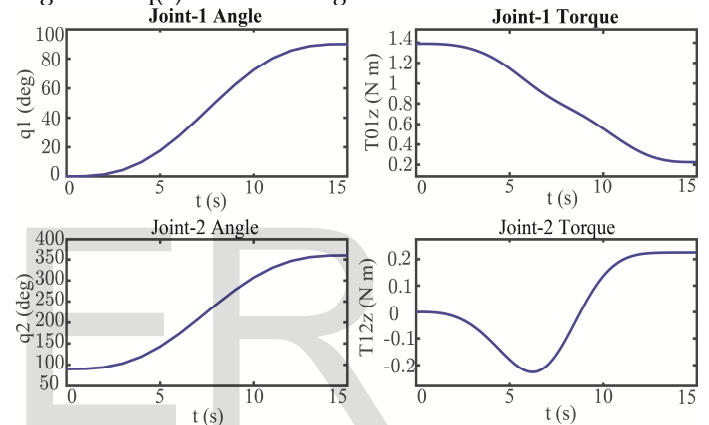Fig. 8. Dynamic Analysis of Two Link Robot Arm, q(1) = 0 ~ 90 degree and q(2) = 90 ~ 360 degree

In Fig. 8, dynamic analysis of 2 links robot arm and q(1) (Joint 1 angle) is setting 0 to 90 degree and q(2) is setting 90 to 360 degree. The initial torque for joint - 1 is near 1.4 N-m and joint – 2 is about 0.22 N-m.

Therefore, the maximum torque of pololu motor is 1.5 N-m is enabled, the above three Fig. 6, Fig. 7, Fig. 8 have maximum torque usage is around 1.55 N-m and 1.6 N-m. This motor selection is suitable for trajectory tracking control system.

3.3 Newton-Euler Formulation

In order to illustrate the use of the N-E equations of motion, the same two-link robot arm with revolute joints as shown in Fig. 4.

All the rotation axes at the joints are along the z-axis perpendicular to the paper surface. The physical dimensions, center of mass, and mass of each link and coordinate systems are given in Table 1.

First, we obtain the rotation matrices from Fig. 4:

$${}^0 R_1 = \begin{bmatrix} C_1 & -S_1 & 0 \\ S_1 & C_1 & 0 \\ 0 & 0 & 1 \end{bmatrix} \; {}^1 R_2 = \begin{bmatrix} C_2 & -S_2 & 0 \\ S_2 & C_2 & 0 \\ 0 & 0 & 1 \end{bmatrix} \; {}^0 R_2 = \begin{bmatrix} C_{12} & -S_{12} & 0 \\ S_{12} & C_{12} & 0 \\ 0 & 0 & 1 \end{bmatrix} \quad (25)$$

$${}^0 R_1 = \begin{bmatrix} C_1 & S_1 & 0 \\ -S_1 & C_1 & 0 \\ 0 & 0 & 1 \end{bmatrix} \; {}^1 R_2 = \begin{bmatrix} C_2 & S_2 & 0 \\ -S_2 & C_2 & 0 \\ 0 & 0 & 1 \end{bmatrix} \; {}^0 R_2 = \begin{bmatrix} C_{12} & S_{12} & 0 \\ -S_{12} & C_{12} & 0 \\ 0 & 0 & 1 \end{bmatrix} \quad (26)$$

We assume the following initial conditions: $\omega_0 = \dot\omega_0 = v_0 = 0$ and $\dot v_0 = (0, g, 0)^T$ with $g = 9.8062$ m/s^2.

Forward equations for $i = 1, 2$. Compute the angular velocity for revolute joint for $i = 1, 2$.

Therefore, for $i = 1$, with $\omega_0 = 0$, we have:

$$^1R_0\omega_1 = {}^1R_0(\omega_0 + z_0\dot\theta_1)$$

$$= \begin{bmatrix} C_1 & S_1 & 0 \\ -S_1 & C_1 & 0 \\ 0 & 0 & 1 \end{bmatrix} \begin{bmatrix} 0 \\ 0 \\ 1 \end{bmatrix}\dot\theta_1 = \begin{bmatrix} 0 \\ 0 \\ 1 \end{bmatrix}\dot\theta_1 \qquad (27)$$

For $i = 2$, we have:

$$^2R_0\omega_2 = {}^2R_1({}^1R_0\omega_1 + z_0\dot\theta_2)$$

$$= \begin{bmatrix} C_2 & S_2 & 0 \\ -S_2 & C_2 & 0 \\ 0 & 0 & 1 \end{bmatrix}\left[\begin{bmatrix} 0 \\ 0 \\ 1 \end{bmatrix}\dot\theta_1 + \begin{bmatrix} 0 \\ 0 \\ 1 \end{bmatrix}\dot\theta_2\right] = \begin{bmatrix} 0 \\ 0 \\ 1 \end{bmatrix}(\dot\theta_1 + \dot\theta_2) \qquad (28)$$

Compute the angular acceleration for revolute joints for $i = 1, 2$.
For $i = 1$, with $\dot\omega_0 = \omega_0 = 0$, we have:

$$^1R_0\dot\omega_1 = {}^1R_0(\dot\omega_0 + z_0\ddot\theta_1 + \omega_0 \times z_0\dot\theta_1) = (0,0,1)^T\ddot\theta_1 \qquad (29)$$

For $i = 2$, we have:

$$^2R_0\dot\omega_2 = {}^2R_1({}^1R_0\dot\omega_1 + z_0\ddot\theta_2 + ({}^1R_0\omega_1)\times z_0\dot\theta_2) = (0,0,1)^T(\ddot\theta_1 + \ddot\theta_2) \qquad (30)$$

Compute the linear acceleration for revolute joints for $i = 1, 2$.
For $i = 1$, with $\dot v_0 = (0, g, 0)^T$, we have:

$$^1R_0\dot v_1 = ({}^1R_0\dot\omega_1)\times({}^1R_0P_1^*) + ({}^1R_0\omega_1)\times[({}^1R_0\omega_1)\times({}^1R_0P_1^*)] + {}^1R_0\dot v_0 \qquad (31)$$

$$= \begin{bmatrix} 0 \\ 0 \\ 1 \end{bmatrix}\ddot\theta_1 \times \begin{bmatrix} 0 \\ 0 \\ 1 \end{bmatrix} + \begin{bmatrix} 0 \\ 0 \\ 1 \end{bmatrix}\dot\theta_1 \times \left\{\begin{bmatrix} 0 \\ 0 \\ 1 \end{bmatrix}\dot\theta_1 \times \begin{bmatrix} 0 \\ 0 \\ 1 \end{bmatrix}\right\} + \begin{bmatrix} gS_1 \\ gC_1 \\ 0 \end{bmatrix}$$

$$= \begin{bmatrix} -l\dot\theta_1^2 + gS_1 \\ l\ddot\theta_1 + gC_1 \\ 0 \end{bmatrix}$$

For $i = 2$, we have:

$$^2R_0\dot v_2 = ({}^2R_0\dot\omega_2)\times({}^2R_0P_2^*) + ({}^2R_0\omega_2)\times[({}^2R_0\omega_2)\times({}^2R_0P_2^*)] \qquad (32)$$
$$+ {}^2R_1({}^1R_0\dot v_0)$$

$$= \begin{bmatrix} 0 \\ 0 \\ \ddot\theta_1 + \ddot\theta_2 \end{bmatrix}\times\begin{bmatrix} 1 \\ 0 \\ 0 \end{bmatrix} + \begin{bmatrix} 0 \\ 0 \\ \dot\theta_1 + \dot\theta_2 \end{bmatrix}\times\left\{\begin{bmatrix} 0 \\ 0 \\ \dot\theta_1 + \dot\theta_2 \end{bmatrix}\times\begin{bmatrix} 1 \\ 0 \\ 0 \end{bmatrix}\right\}$$

$$+ \begin{bmatrix} C_2 & S_2 & 0 \\ -S_2 & C_2 & 0 \\ 0 & 0 & 1 \end{bmatrix}\begin{bmatrix} -l\dot\theta_1^2 + gS_1 \\ l\ddot\theta_1 + gC_1 \\ 0 \end{bmatrix}$$

$$= \begin{bmatrix} l(S_2\ddot\theta_2 - C_2\dot\theta_1^2 - \dot\theta_1^2 - \dot\theta_2^2 - 2\dot\theta_1\dot\theta_2) + gS_{12} \\ l(\ddot\theta_1 + \ddot\theta_2 + C_2\ddot\theta_1 + S_2\dot\theta_1^2) + gC_{12} \\ 0 \end{bmatrix}$$

Compute the linear acceleration at the center of mass for links 1 and 2:
For $i = 1$, we have:

$$^1R_0\bar a_1 = ({}^1R_0\dot\omega_1)\times({}^1R_0\bar s_1) + ({}^1R_0\omega_1)\times[({}^1R_0\omega_1)\times({}^1R_0\bar s_1)] + {}^1R_0\dot v_1 \qquad (33)$$

Where

$$\bar s_1 = \begin{bmatrix} -\frac{1}{2}C_1 \\ -\frac{1}{2}S_1 \\ 0 \end{bmatrix} \qquad {}^1R_0\bar s_1 = \begin{bmatrix} C_1 & S_1 & 0 \\ -S_1 & C_1 & 0 \\ 0 & 0 & 1 \end{bmatrix}\begin{bmatrix} -\frac{1}{2}C_1 \\ -\frac{1}{2}S_1 \\ 0 \end{bmatrix} = \begin{bmatrix} -\frac{1}{2} \\ 0 \\ 0 \end{bmatrix}$$

Thus,

$$^1R_0\bar a_1 = \begin{bmatrix} 0 \\ 0 \\ 1 \end{bmatrix}\ddot\theta_1 \times \begin{bmatrix} -\frac{1}{2} \\ 0 \\ 0 \end{bmatrix} + \begin{bmatrix} 0 \\ 0 \\ \dot\theta_1 \end{bmatrix}\times\left\{\begin{bmatrix} 0 \\ 0 \\ \dot\theta_1 \end{bmatrix}\times\begin{bmatrix} -\frac{1}{2} \\ 0 \\ 0 \end{bmatrix}\right\} + \begin{bmatrix} -l\dot\theta_1^2 + gS_1 \\ l\ddot\theta_1 + gC_1 \\ 0 \end{bmatrix}$$

$$= \begin{bmatrix} -\frac{1}{2}\dot\theta_1^2 + gS_1 \\ \frac{1}{2}\ddot\theta_1 + gC_1 \\ 0 \end{bmatrix}$$

For $i = 2$, we have:

$$^2R_0\bar a_2 = ({}^2R_0\dot\omega_2)\times({}^2R_0\bar s_2) + ({}^2R_0\omega_2)\times[({}^2R_0\omega_2)\times({}^2R_0\bar s_2)] + {}^2R_0\dot v_2 \qquad (34)$$

Where

$$\bar s_2 = \begin{bmatrix} -\frac{1}{2}C_{12} \\ -\frac{1}{2}S_{12} \\ 0 \end{bmatrix} \qquad {}^2R_0\bar s_2 = \begin{bmatrix} C_{12} & S_{12} & 0 \\ -S_{12} & C_{12} & 0 \\ 0 & 0 & 1 \end{bmatrix}\begin{bmatrix} -\frac{1}{2}C_{12} \\ -\frac{1}{2}S_{12} \\ 0 \end{bmatrix} = \begin{bmatrix} -\frac{1}{2} \\ 0 \\ 0 \end{bmatrix}$$

Thus,

$$^2R_0\bar a_2 = \begin{bmatrix} 0 \\ 0 \\ \ddot\theta_1 + \ddot\theta_2 \end{bmatrix}\times\begin{bmatrix} -\frac{1}{2} \\ 0 \\ 0 \end{bmatrix} + \begin{bmatrix} 0 \\ 0 \\ \dot\theta_1 + \dot\theta_2 \end{bmatrix}\times\left\{\begin{bmatrix} 0 \\ 0 \\ \dot\theta_1 + \dot\theta_2 \end{bmatrix}\times\begin{bmatrix} -\frac{1}{2} \\ 0 \\ 0 \end{bmatrix}\right\}$$

$$+ \begin{bmatrix} l(S_2\ddot\theta_1 - C_2\dot\theta_1^2 - \dot\theta_1^2 - 2\dot\theta_1\dot\theta_2) + gS_{12} \\ l(\ddot\theta_1 + \ddot\theta_2 + C_2\ddot\theta_1 + S_2\ddot\theta_2) + gC_{12} \\ 0 \end{bmatrix}$$

$$= \begin{bmatrix} l(S_2\ddot\theta_1 - C_2\dot\theta_1^2 - \frac{1}{2}\dot\theta_1^2 - \frac{1}{2}\dot\theta_2^2 - \dot\theta_1\dot\theta_2) + gS_{12} \\ l(C_2\ddot\theta_1 + S_2\dot\theta_1^2 + \frac{1}{2}\ddot\theta_1 + \frac{1}{2}\ddot\theta_2 + gC_{12}) \\ 0 \end{bmatrix}$$

Backward equations for $i = 2, 1$. Assuming no-load conditions, $f_3 = n_3 = 0$. We compute the force exerted on link - i for $i = 2, 1$.
For $i = 2$, with $f_3 = 0$, we have:

$$^2R_0f_2 = {}^2R_3({}^3R_0f_3) + {}^2R_0F_2 = {}^2R_0F_2 = m_2{}^2R_0\bar a_2 \qquad (35)$$

$$= \begin{bmatrix} m_2l(S_2\ddot\theta_1 - C_2\dot\theta_1^2 - \frac{1}{2}\dot\theta_1^2 - \frac{1}{2}\dot\theta_2^2 - \dot\theta_1\dot\theta_2) + gm_2S_{12} \\ m_2l(C_2\ddot\theta_1 + S_2\dot\theta_1^2 + \frac{1}{2}\ddot\theta_1 + \frac{1}{2}\ddot\theta_2) + gm_2C_{12} \\ 0 \end{bmatrix}$$

For $i = 1$, we have:

$$^1R_0f_1 = {}^1R_2({}^2R_0f_2) + {}^1R_0F_1 \qquad (36)$$

$$= \begin{bmatrix} C_2 & -S_2 & 0 \\ S_2 & C_2 & 0 \\ 0 & 0 & 1 \end{bmatrix} \begin{bmatrix} m_2 l(S_2\ddot{\theta}_1 - C_2\dot{\theta}_2 - \frac{1}{2}\dot{\theta}_1^2 - \frac{1}{2}\dot{\theta}_2^2 - \dot{\theta}_1\dot{\theta}_2) + gm_2 S_{12} \\ m_2 l(C_2\ddot{\theta}_1 + S_2\dot{\theta}_1^2 + \frac{1}{2}\ddot{\theta}_1 + \frac{1}{2}\ddot{\theta}_2) + gm_2 C_{12} \\ 0 \end{bmatrix} + m_1 {}^1R_0\bar{a}_1$$

$$= \begin{bmatrix} m_2 l[-\dot{\theta}_1^2 - \frac{1}{2}C_2(\dot{\theta}_1^2 + \dot{\theta}_2^2) - C_2\dot{\theta}_1\dot{\theta}_2 - \frac{1}{2}S_2(\ddot{\theta}_1 + \ddot{\theta}_2)] \\ -m_2 g(C_{12}S_2 - C_2 S_{12}) - \frac{1}{2}m_1 l\dot{\theta}_1^2 + m_1 gS_1 \\ m_2 l[\ddot{\theta}_1 - \frac{1}{2}S_2(\dot{\theta}_1^2 + \dot{\theta}_2^2) - S_2\dot{\theta}_1\dot{\theta}_2 + \frac{1}{2}C_2(\ddot{\theta}_1 + \ddot{\theta}_2)] \\ + m_2 gC_1 + \frac{1}{2}m_1 l\ddot{\theta}_1 + m_1 gC_1 \\ 0 \end{bmatrix}$$

Compute the moment exerted on link - i for $i = 2, 1$.
For $i = 2$, with $n_3 = 0$. we have:

$$ {}^2R_0 n_2 = ({}^2R_0 p_2^* + {}^2R_0 \bar{s}_2) \times ({}^2R_0 F_2) + {}^2R_0 N_2 \qquad (37)$$

Where

$$p_2^* = \begin{bmatrix} lC_{12} \\ lS_{12} \\ 0 \end{bmatrix} \quad {}^2R_0 p_2^* = \begin{bmatrix} C_{12} & S_{12} & 0 \\ -S_{12} & C_{12} & 0 \\ 0 & 0 & 1 \end{bmatrix} \begin{bmatrix} lC_{12} \\ lS_{12} \\ 0 \end{bmatrix} = \begin{bmatrix} l \\ 0 \\ 0 \end{bmatrix}$$

Thus,

$$ {}^2R_0 n_2 = \begin{bmatrix} \frac{1}{2} \\ 0 \\ 0 \end{bmatrix} \times \begin{bmatrix} m_2 l(S_2\ddot{\theta}_1 - C_2\dot{\theta}_2 - \frac{1}{2}\dot{\theta}_1^2 - \frac{1}{2}\dot{\theta}_2^2 - \dot{\theta}_1\dot{\theta}_2) + gm_2 S_{12} \\ m_2 l(C_2\ddot{\theta}_1 + S_2\dot{\theta}_1^2 + \frac{1}{2}\ddot{\theta}_1 + \frac{1}{2}\ddot{\theta}_2) + gm_2 C_{12} \\ 0 \end{bmatrix}$$

$$+ \begin{bmatrix} 0 & 0 & 0 \\ 0 & \frac{1}{12}m_2 l^2 & 0 \\ 0 & 0 & \frac{1}{12}m_2 l^2 \end{bmatrix} \begin{bmatrix} 0 \\ 0 \\ \ddot{\theta}_1 + \ddot{\theta}_2 \end{bmatrix}$$

$$= \begin{bmatrix} 0 \\ 0 \\ \frac{1}{3}m_2 l^2\ddot{\theta}_1 + \frac{1}{3}m_2 l^2\ddot{\theta}_2 + \frac{1}{2}m_2 l^2(C_2\ddot{\theta}_1 + S_2\dot{\theta}_1^2) + \frac{1}{2}m_2 glC_{12} \end{bmatrix}$$

For $i = 1$, we have:

$$ {}^1R_0 n_1 = {}^1R_2[{}^2R_0 n_2 + ({}^2R_0 p_1^*) \times ({}^2R_0 f_2)] \\ + ({}^1R_0 p_1^* + {}^1R_0 \bar{s}_1) \times ({}^1R_0 F_1) + ({}^1R_0 N_1) \qquad (38)$$

Where

$$p_1^* = \begin{bmatrix} lC_1 \\ lS_1 \\ 0 \end{bmatrix} \quad {}^2R_0 p_1^* = \begin{bmatrix} lC_2 \\ -lS_2 \\ 0 \end{bmatrix} \quad {}^1R_0 p_1^* = \begin{bmatrix} l \\ 0 \\ 0 \end{bmatrix}$$

Thus,

$$ {}^1R_0 n_1 = {}^1R_2({}^1R_0 n_2) + {}^1R_2[({}^2R_0 p_1^*) \times ({}^2R_0 f_2)] \\ + [\frac{1}{2}, 0, 0]^T \times ({}^1R_0 F_1) + ({}^1R_0 N_1)$$

Finally, we obtain the joint torques applied to each of the joint actuators for both links.
For $i = 2$, with $b_2 = 0$, we have:

$$\tau_2 = ({}^2R_0 n_2)^T ({}^2R_1 z_0)$$
$$= \frac{1}{3}m_2 l^2\ddot{\theta}_1 + \frac{1}{3}m_2 l^2\ddot{\theta}_2 + \frac{1}{2}m_2 l^2 C_2\ddot{\theta}_1$$
$$+ \frac{1}{2}m_2 glC_{12} + \frac{1}{2}m_2 l^2 S_2\dot{\theta}_1^2 \qquad (39)$$

For $i = 1$, with $b_1 = 0$, we have:

$$\tau_1 = ({}^1R_0 n_1)^T ({}^1R_0 z_0)$$
$$= \frac{1}{3}m_1 l^2\ddot{\theta}_1 + \frac{4}{3}m_2 l^2\ddot{\theta}_1 + \frac{1}{3}m_2 l^2\ddot{\theta}_2 + m_2 C_2 l^2\ddot{\theta}_1$$
$$+ \frac{1}{2}m_2 l^2 C_2\ddot{\theta}_2 - m_2 S_2 l^2\dot{\theta}_1\dot{\theta}_2 - \frac{1}{2}m_2 S_2 l^2\dot{\theta}_2^2 \qquad (40)$$
$$+ \frac{1}{2}m_1 glC_1 + \frac{1}{2}m_2 glC_{12} + m_2 glC_1$$

4 FRICTION IDENTIFICATION

Mostly, position control system based on the conventional Proportional-Integral-Derivative (PID) method. The conventional Proportional-Integral-Derivative (PID) equation is as followed:

$$u_{PID} = Ke(t) + L\int e(t)dt + B\frac{de(t)}{dt} \qquad (41)$$

Where u_{PID} is the controller output from the controller and K, L and B are positive real numbers, which represent the proportional, integral and derivative gains. The $e(t)$ is define as $p(t)$ (actual position) that is subtracted from p_d(t) (desired position).

4.1 Rate Depended Friction Identification

For the friction compensation, it is required Polou DC motor with two channels linear quadrature encoder and 100:1 gear transmission, arm at the motor sharft and basement for fixing the motor in it. Motor is driven by L298N driver with 12V DC.

For the control algorithm, it is used LPC 1768, ARM based Cortex-M3 microcontroller, the clock frequency is 96 MHz. The ARM microcontroller has many timers and serial connectors. Personal computer (PC) is used for serial monitoring and programming for microcontroller.
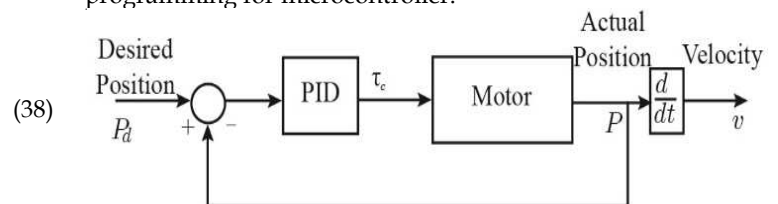

Fig. 9. Position Control Block Diagram for Friction Identifition Experiment

Friction model allows different parameter sets for positive and negative velocity regime and easily identifiable parameters. The model clearly separates the high and low velocity regime. It can easily be implemented and introduced in real time control algorithms. This experiment (see Fig. 9) is finding the parameters that actually appear from the friction force (passive) in gear box of the motor and friction in motor (electro-mechanical device has friction).
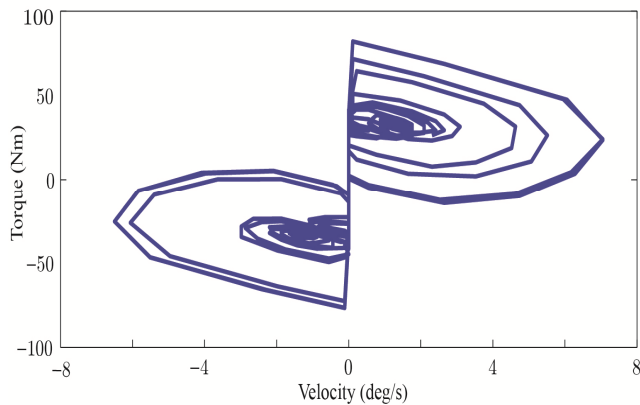
Fig. 10. Torque and Velocity Curve to identify the friction force

This Curve is Torque and Velocity Curve to identify the friction force as shown in Fig. 10. Because Friction is a Function of Velocity.

When the motor is feed sinusoidal input in Fig. 9, the motor genate speed and torque and that is put on the coordinate system in Fig. 10. The data from Fig. 10 is divided by two and this data is stored in Matlab software. After that Fig. 11 is generated from this storage data.

According to the Fig. 11, static friction F_s can be seen in vertical positive and negative peak point of red line. F_s is greater than the other frictions magnitude. Static friction is also depending on the velocity that is at zero condition, at that time static friction force appears.
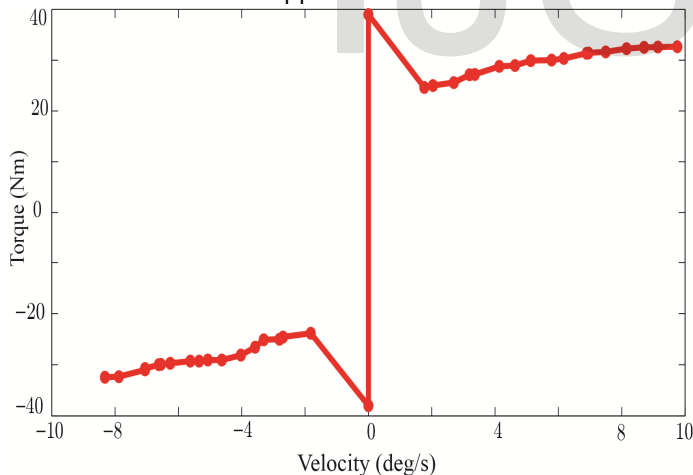

Fig. 11. This Curve is the Rate-Depended Friction Identification Curve. Friction Parameter is Received from this Curve.

4.1 Modeling of Friction Compensator

Friction is the important part for control system in high quality precision mechanisms, electro-mechanical devices, hydraulic and pneumatic system. Due to the effect of friction, the control system does not reach the desired position, to solve this problem, the control engineer used higher gain control loops, that is not better choice, inherently require a suitable friction model to compensate and still in precise position. A good model is also required to analyse stability, find controller gain and perform stimulation.

This paper presents an encoder-based friction compensator for a geared actuator. The compensator only requires the encoder signal as its input to enhance the system.

Most of existing friction compensation techniques are based on friction models that uses the velocity as its input. It can be seen in Fig. 13. The friction can be found at low velocity that is from derivative of the position of the encoder. In this saturation, the system meets with static friction state, being sensitive to external force. When the velocity is more and more, the compensator produces a force to cancel the friction force based on a predefined rate at friction model.

TABLE 2
PARAMETER VALUES OBTAINED FROM FIG. 11

Parameter	F_{s+}	F_{c+}	F_{v+}	v_{s+}	F_{s-}	F_{c-}	F_{v-}	v_{s-}
Unit	N-m	N-m	N-m	deg/s	N-m	N-m	N-m	deg/s
Value	39	24.61	1	1.765	38	23.89	1.326	1.82

The proposed friction model is as followed:

$$F_f = (F_c + (F_s - F_c)e^{-\frac{|v|}{v_s}})sign(v) + F_v v \qquad (42)$$

Where F_s, F_c, F_v, is the Static, Coulomb, Viscous friction and v_s is the Stribeck velocity. δ is an additional empirical parameter. v is the velocity estimated from encoder. Table 2 parameter values in friction model eq. (42).

5 EXPERIMENTAL RESULT

This section presents the results of experiments showing the effectiveness of the proposed PID and PID with friction control scheme are illustrated by using a two link robot(2-DOF) positioning system. The performance of the proposed controller is compared with a PID with friction compensator. For this experiment, it is required two sets of Polou DC motor with two channels linear quadrature encoder and 100:1 gear transmission. Motor is driven by L298N driver with 12V DC. For the control algorithm, it is used NXP LPC 1768, the clock frequency is 96 MHz. The microcontroller is connected to a PC computer through USB cable. The PC is used for data monitoring and acquisition by Cool Term Serial Data Logger. The encoder resolution is 65.33 pulses per revolution and entire resolution of the motor shaft is 6533 pulses per revolution.
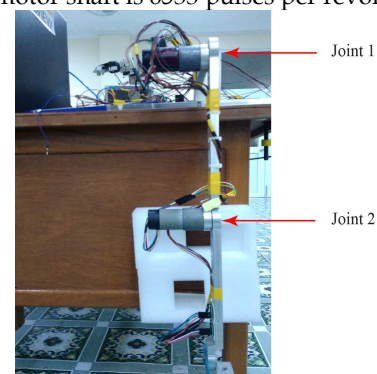

Fig. 12. Experimental Setup of the 2-Links Robot Arm

5.1 Proposed Position Controller

The proposed position controller is the combination of the convential PID controller with friction compensator. The controller block diagram is expressed in Fig. 13.
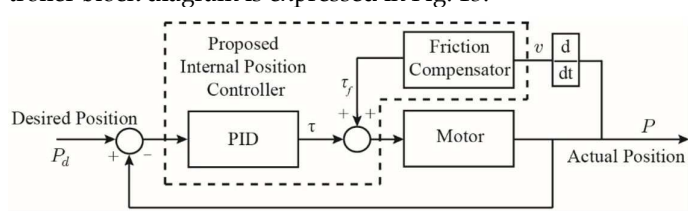

Fig. 13. Proposed Position Controller Block Diagram

5.1 Set Point and Trajectory Tracking Control with PID

To validate the proposed framework, following experimental steps were passed through step by step. The first step of experiment is PID gain turning for Joint – 1. To do this gain turning, we had to set desired input (blue line) by step or set-point input (this is shown in Fig. 14 and Fig. 15) in following block diagram. Gain turning was trial and error method. Trial and error method is easy.
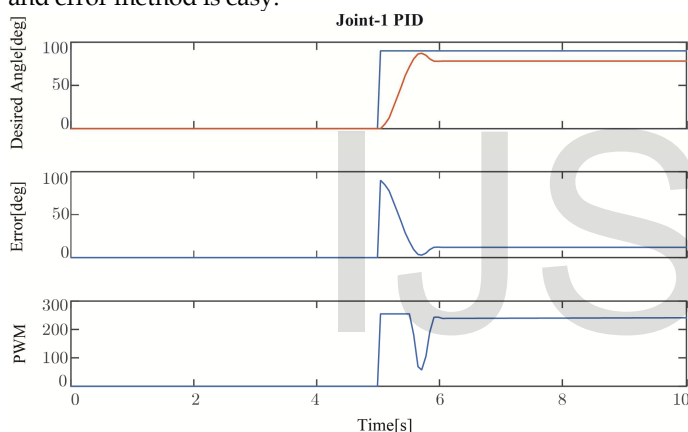

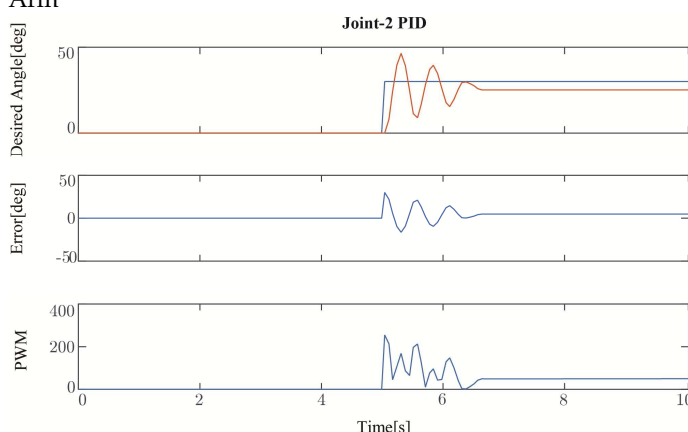Fig. 14. PID Set Point Control Result of Joint 1 of 2-Links Robot Arm

Fig. 15. PID Set Point Control Result in Joint 2 of 2-Links Robot Arm

The first experiment was the gain turning for Joint – 1 PID controller in Fig. 14. Here, desired input was setting up at 60 degree, the controller had error input at this condition because actual angle is less than desired angle. The controller pro-

duced the torque command that was equal to the product of K_p and error value. In this condition, the K_p gain was increase to reach the appropriate torque, however, K_p turning was stopped when the actual angle beyond the desired angle. The condition beyond the desired angle was called overshoot region. This overshoot effect was recovered by the derivative gain K_d, was turned to reduce the actual angle to reach the desired angle, however, the actual angle decreased under the actual angle which was called undershoot. To compensate the undershoot effect, the K_i was turned to reach desired angle. Integral turning, absolutely based on sampling interval. Although, integral term did not recover the steady-state region. Friction compensator was used together with PID controller and it could recover steady-state error even when the sampling frequency is low. PID Gain value is seen in Table 3.

TABLE 3
Parameter of PID Controller

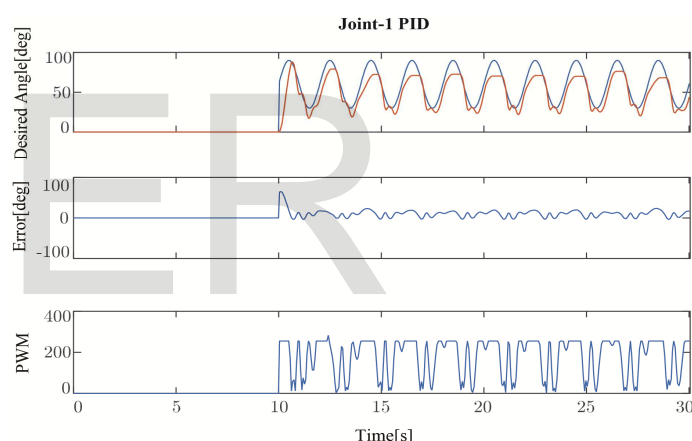| PID Paremeter	Gain
K_p	10
K_i	0.05
K_d	0.05

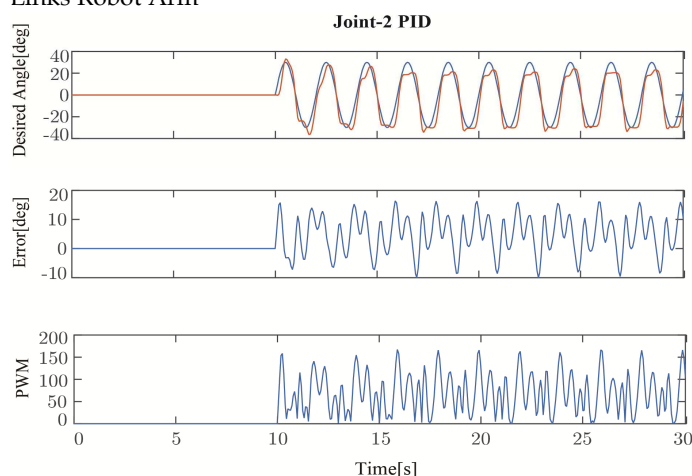Fig. 16. PID Trajectory Tracking Control Result in Joint 1 of 2-Links Robot Arm

Fig. 17. PID Trajectory Tracking Control Result in Joint 2 of 2-Links Robot Arm

In Fig. 14, the maximum joint torque was produced in

transient region, PWM is 100 percent ON [255 units i.e. Arduino PWM value]. At this transient region, PID must be overshoot but it reached near the desired angle. Joint 1 did not reach the desired angle in steady state region.

In Fig. 15, the maximum joint torque was produced in transient region, PWM is almost 100 percent ON [255 units i.e. Arduino PWM value.] At this transient region, PID had overshoot. Derivative term reduced the overshoot but it caused the undershoot. Joint 2 reached near desired angle in steady state region but integral term did not fully recover in steady state region. Therefore, friction compensation for joint 1 and 2 were shown in Fig. 18 and Fig. 19.

5.2 Set Point and Trajectory Tracing Control with PID + Friction Compensator

Fig. 16. and Fig. 18 PID trajectory tracking control result and PID with friction compensator result in joint 1 of robot arm did not follow the desired trajectory. To answer this question, inverse dynamic analysis of 2 links robot arm results is shown in Fig. 6, Fig. 7 and Fig. 8.
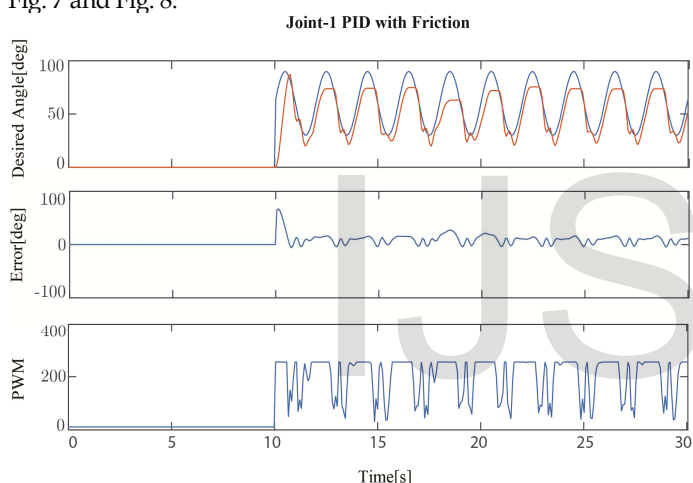

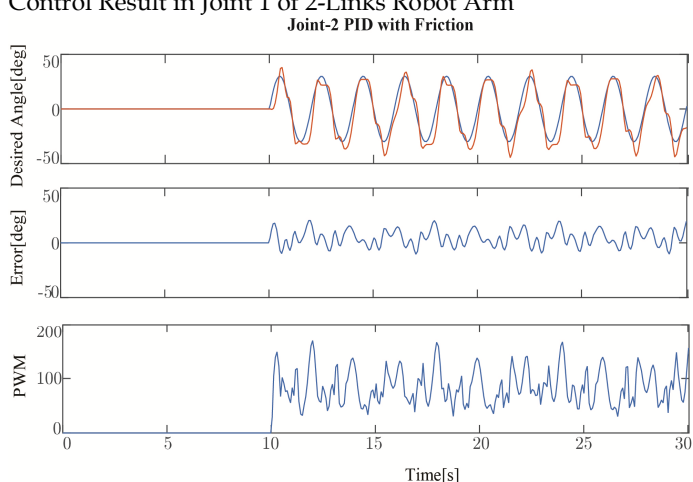Fig. 18. PID + Friction Compensator with Trajectory Tracking Control Result in Joint 1 of 2-Links Robot Arm

Fig. 19. PID + Friction Compensation with Trajectory Tracking Result in Joint 2 of Two Links Robot Arm

6 DISCUSSION

Forward kinematic and Inverse Kinematic are interned to Admittance type force controller and dynamic and inverse dynamic are formulated by the Newton-Euler and Lagrange.

This paper explains briefly the differences of the formulations, and then analyzes the Lagrange method in Matlab. The corresponding joint torques computed in each time step are plotted. Initially, the end effector motions are used to obtain the computed torque result in trajectory, consider the appropriate motor selection for two links. It is proposed to use this arm for following a desired trajectory by using an PID control with friction compensator. A prototype is made with metal links and motors. This system with NXP LPC 1768 microcontroller board is employed to drive the servos in incremental encoder as per the tracking point and its inverse kinematics intern to Admittance type control system for future work. Finally, to illustrate the control system on the prototype and dynamic analysis is presented.

Current control DC servo motor should also be recommended for future work. If the torques can also be measured, for example by measuring the current, it is actually possible to compute the friction parameters explicitly by friction identification method. Now, friction identification is drawn by PWM vs Velocity. The model in this paper is also limited in other aspects. A perfect model would contain dynamic effects like joint friction, and there would be bounds on the maximum input torque for the motors. Therefore, PID controller is added by friction compensator; however, it could not reach the desired trajectory. The motor speed should be increase because the experimental result by trajectory tracking was tasted by 0.5 Hz.

7 CONCLUSION

In this paper, the dynamics analysis of the two links robot arm and the proposed position controller are presented. Dynamic analysis is formulated by using the Newton-Euler and Lagrangian methods and the dynamic analysis is also presented by Lagrangian method. The computed corresponding joint torques are plotted. From this result, the motor is choosen. It is used in robot arm for following a desired trajectory by using PID (proportional, integral and derivative) control with friction compensator. The friction compensator is integrated with static friction, Coulomb friction, viscous friction and Stribeck effect. Moreover, the proposed (PID plus friction compensator) controller minimize the position error in set point control and trajectory tracking control compare with convention PID one, and thus, improve the stability.

REFERENCES

[1] W. Huo, S. Mohammed, J. C. Moreno, and Y. Amirat, "Lower limb wearable robots for assistance and rehabilitation: A state of the art," 2014.

[2] K. Kiguchi, T. Tanaka, and T. Fukuda, "Neuro-fuzzy control of a robotic exoskeleton with EMG signals," *IEEE Trans. Fuzzy Syst.*, vol. 12, no. 4, pp. 481–490, Aug. 2004.

[3] R. Song, K. Yu Tong, X. Hu, and L. Li, "Assistive control system using continuous myoelectric signal in robot-aided arm training for patients after stroke," *IEEE Trans. Neural Syst. Rehabil. Eng.*, vol. 16, no. 4, pp. 371–379, Aug. 2008.

[4] Fernando Reyes, Rafael Kelly, "Experimental evaluation of model-based controllers on a direct-drive robot arm", *Mechatronics*, Vol. 11, P.P. 267-282, 2001

[5] Jolly Shah, S.S. Rattan, B.C. Nakra, "Kinematic Analysis of 2-DOF Planer Robot Using Artificial Neural Network", *World Academy of Science*, Engineering and Technology, Vol. 81, pp. 282-285, 2011

[6] Tarcisio A.H. Coelho, Liang Yong, Valter F.A. Alves, "Decoupling of dynamic equations by means of adaptive balancing of 2-dof open-loop mechanisms", Mechanism and Machine Theory 39, (2004), 871–881

[7] B.K. Rout, R.K. Mittal, "Parametric design optimization of 2-DOF R–R planar manipulator- A design of experiment approach", *Robotics and Computer-Integrated Manufacturing*, 24 (2008) 239–248

[8] Vigen Arakelian, Jean-Paul Le Baron, Pauline Mottu, "Torque minimization of the 2-DOF serial manipulators based on minimum energy consideration and optimum mass redistribution", *Mechatronics*, 21 (2011) 310–314

[9] Ravindra Biradar, M.B. Kiran, "The Dynamics of Fixed Base and Free-Floating Robotic Manipulator", *International Journal of Engineering Research & Technology*, Vol. 1 (5), 2012, 1-9

[10] M W Spong, "On the robust control of robot manipulators". *IEEE Transactions on Automatic Control*, Vol. 37(11), P.P. 1782-86, 1992

[11] Yoshikawa T., "Manipulability of robotic mechanisms", *The International Journal of Robotics Research*, 4, 1985, No 2, 3-9.

[12] L. Márton, "On analysis of limit cycles in positioning systems near Striebeck velocities," Mechatronics, vol. 18, pp. 46-52, 2008.

[13] P.R. Dahl, "A solid friction model," DTIC Document1968.

[14] Canudas de Wit, C., Olsson, H., Astrom, K., and Lischinsky, P., 1995, "A New Model for Control of Systems with Friction," IEEE Trans. Autom. Control, 40(3), pp. 419–425.

[15] Al-Bender, F., Lampaert, V., and Swevers, J., 2005, "The Generalized Maxwell-Slip Model: A Novel Model for Friction Simulation and Compensation," IEEE Trans. Autom. Control, 50(11), pp. 1883–1887.

[16] M. T. S. Aung, R. Kikuuwe, and M. Yamamoto, 2015, "Friction compensation of geared actuators with high presliding stiffness," *Trans. ASME, J. Dyn. Syst., Meas., Contr.*, vol. 137, no. 1, p. 011007.